Heinz Hugli*
Werner Frei
Institute for Physics and Imaging Science
University of Southern California
Marina del Rey, CA 90291

Understanding Anisotropic Reflectance in Mountainous Terrain

Radiance, which depends upon target reflectance characteristics and the geometry of incident and reflected rays, is fully described by the bidirectional reflectance distribution function (BRDF).

INTRODUCTION

How to go from raw radiance data to useful information regarding surface cover is an important topic of remote sensing. Raw images exhibit a radiometry which is determined by various physical factors and must, therefore, be corrected for the unwanted factors in order to be quantita-

Multitemporal remote sensing is used to survey physical and biological processes on the Earth surface. Such processes are made apparent by detecting changes which occurred between images taken at different times. Computerized image change detection has several advantages over classical photointerpretation in performing this task (Frei *et al.*, 1980). Unfortunately, it is also sensi-

ABSTRACT: *In remote sensing radiometry captures the aggregate effect of a number of physical factors. Typically, most of these must be factored out using radiometric corrections in order to obtain the information of interest. Here the question of anisotropic reflectance in mountainous terrain is analyzed. The paper is divided into four parts. First, an overview of known methods is given. Second, a remote sensing model and a quantitative analysis of radiometric correction in mountainous terrain is presented. Simple radiometric effects are explained. Third, a computer simulation is performed in order to better understand the combined effect of anisotropic reflectance characteristics and variable surface orientations, which are the properties of mountainous terrain covered with vegetation. The results illustrate the mechanisms of typical radiometric effects and show that the possibilities for modeling reflectance are limited. This limitation is due to the practical difficulty of determining exactly all the reflection properties in a mountainous environment. Fourth, as a practical approach to the correction, a reflection model is proposed, which considers the particularities of airborne remote sensing in mountainous terrain.*

tively useful. Radiometric correction methods have been investigated since the beginning of remote sensing; most efforts have been concerned with the common purpose of improving the accuracy of remote measurements of surface reflection properties such as albedo (Reeves *et al.*, 1975; Lintz and Simonett, 1976). The need for radiometric correction methods is illustrated here by the practical difficulties encountered in the detection of change in a set of multitemporal images.

* Now with the Institut de Microtechnique, Universite de Neuchatel, Maladiere 71, CH-2000 Neuchatel, Switzerland.

tive to changes not related to the processes of interest. Such changes include different recording conditions of subsequent images, for example, illumination and viewing conditions, characteristics of the atmosphere, as well as characteristics of the sensor.

Of course, in the ideal case all images of a multitemporal image set would be taken under exactly the same recording conditions. This would result in images differing only by the amount of physical or biological changes that have occurred on the Earth surface. This is unfortunately not possible in most practical applications, i.e., where the illumination is very different because the images to be

compared are taken at different times of the year, where the sensor location is different for flight, and where neither the atmospheric nor the sensor characteristics are constant.

In the basic approach to this problem, ground reflectance is considered to be the useful information whereas other factors are unwanted effects which must be factored out. In this approach, the estimation of reflectance distribution plays a major role. It is analyzed here for anisotropic reflectances in mountainous terrain with special emphasis on low altitude remote sensing.

This paper is organized in four parts. The first part gives the background of radiometric correction. We overview its various aspects and review at the same time the results obtained in that field. This suggests that specific approaches are required in mountainous terrain. In the second part we present a complete analysis of radiometry in remote sensing of flat and mountainous terrain. This is done analytically by modeling the remote sensing process. Special attention is given to the reflectance characteristic of the ground. Several anisotropic reflection models known in the literature are first compared and then used to explain the main radiometric mechanisms. In the third part the analysis is performed numerically and the results are presented in the form of a computer simulation that illustrates radiometric effects such as hot and specular spots in flat and in mountainous terrain. This analysis reveals that vegetated surfaces in mountainous terrain require a more complex model than those now available. The form of such a model is suggested, but it is believed to be too complex to be of practical use. In the last part, as a practical approach to correction, a reflection model is proposed for correcting airborne remotely sensed images of mountainous terrain.

BACKGROUND

In this section we review the various aspects of radiometric correction in remote sensing and suggest that specific approaches are required in mountainous terrain, especially for wide-angle imagery.

REFLECTION PROPERTIES

Reflection properties of the ground are the heart of the correction problem. Any correction method uses some *a priori* knowledge of the reflection properties of the surface of interest, i.e., a reflection model. The correction accuracy is then basically limited by the discrepancy between model and reality.

Practically, a reflection model describes the reflectance variations of a reflecting surface, and it is quantitatively described by the reflectance characteristic.

A diffuse reflection model or Lambert reflector is a good average approximation of the reflection characteristic of the solid part of the Earth's surface. For this reason, and also because of its simple mathematical form, this model is used routinely for radiometric corrections (Richason, 1978; Robinove and Chavez, 1978; Sjoberg and Horn, 1980). Alas, the diffuse model is only a rough approximation if specific portions of the Earth's surface are considered separately. With the exception of areas covered with loose sand or fresh fallen snow (Middleton and Mungall, date?), most of the Earth's surface has anisotropic reflection properties. Water and glassy snow are typical forwardscatters whereas volcanic rocks (Hapke and Horn, 1963) and plowed fields (Eaton and Dirmhin, 1979) are typical backscatters. Reflection models exist for both typical forwardscatter and typical backscatter types. Forwardscattering was analyzed extensively in connection with the search for an explanation of the radiometric behavior of the moon (Minnaert, 1961; Hapke, 1963). These studies resulted in a backscatter reflection model which, if it fits the moon better than the Earth, gives nevertheless a good insight in the reflection process responsible for the backscattering.

The other typical model, the forwardscatter or specular reflection model, resulted from measurements on snow and metallic surfaces and is known as the Torrance-Sparrow model (Torrance and Sparrow, 1967; Trowbridge and Reitz, 1975; Blinn, 1977).

More complex and less predictable are the reflectance characteristics of vegetated surfaces. Their complexity is a direct consequence of the geometric structure which determines barely predictable shadow patterns causing reflectance anisotropy. The use of the Duntley equations (Allen *et al.*, 1970; Suits, 1972; Reeves *et al.*, 1975) as a reflection model has been abandoned for a more systematic approach based on measurements of the reflectance characteristics of all important vegetated canopies likely to be encountered in aerial images (Eaton and Dirmhin, 1979; Kriebel, 1978). These measurements permit one to build a numerical reflection model. The advantage of a numerical model is its ability to model reflectance behaviors of arbitrary complexity. It is a very efficient tool for it can be used as a model of reflection for image synthesis, or alternatively, for image analysis, as a means for comparing different canopies or as a means for measuring the degree of radiometric homogeneity within a given canopy (Kimes and Kirchner, 1981; Kimes *et al.*, 1980). Finally, another reflection model based on a diffuse surface perturbed by either spheres or cylinders has been analyzed and proposed as a practical model for vegetated surfaces (Egbert, 1977).

ATMOSPHERE

Atmospheric effects are extremely variable. Under good visibility conditions, a usable atmospheric model can be set up which predicts the

attenuation factor of a given light path as well as the amount and distribution of the scattered light responsible for the skylight (RCA, 1974; Tricker, 1970; Divari, 1970; Ahern *et al.*, 1978). The difficulty arises from the fact that the atmosphere and the ground are interacting, with the consequence that the skylight is not only a function of the sun and the atmosphere, but is also dependent both on the reflectance properties of the ground (Koepke and Kriebel, 1978) and on its topographic shape (Kimes and Kirchner, 1981). Thus, an independent analysis of the light processes both in the atmosphere and on the ground is generally not possible. Only under certain circumstances (Favre *et al.*, 1979) can both processes be analyzed separately. For example, a constant skylight and a simple distribution function have been used with success in previous practical applications (Sjoberg and Horn, 1980).

SENSOR

Traditionally, the recording is photographic. As a measuring device, the camera, film, and film-scanner make it difficult to control radiometric characteristics. The sensor transfer characteristic is non-linear overall, spatially variable, and variable from film batch to film batch. It must be compensated by the use of anti-vignetting filters and by adequate radiometric calibration methods using greyscales directly exposed onto the film (Walker, 1979) or reference reflectors in the imaged scene (Egbert, 1977).

Recording by electro-optical scanners is more recent. This method shows a stable and linear sensor characteristic. For radiometric measurements, the use of electro-optic scanners is therefore preferable if available.

HIGH VERSUS LOW ALTITUDE IMAGERY

High altitude or spacecraft imagery and low altitude or aerial imagery do not give rise to the same difficulty for radiometric corrections. This is due to the particularities of the reflectance characteristic and to the fact that the visual angle under which the images are taken is usually small for high altitude images whereas it is large for low altitude images. As a consequence, more important reflectance variations are usually found in low altitude imagery. As a remedy, methods have been proposed in the special case of flat terrain: the anisotropy was either reduced by reducing the visual angle (Walker, 1979), or compensated for its major effect, i.e., the hot spot produced by strong backscattering (Nagao, 1977), or corrected according to a complex reflection model (Egbert, 1977).

FLAT VERSUS MOUNTAINOUS SITES

In all applications and models considered so far, the ground was considered flat. In mountainous terrain, the problem is more complex. Here, indeed, radiometry is the consequence of the combined effect of reflection properties and surface orientation (Holben and Justice, 1980). The radiometric correction method for flat sites must, therefore, be modified to also account for the variable surface orientation.

A particular approach exists in the case of a small viewing angle, i.e., high altitude imagery, where the assumption of parallel observation rays can be made with the consequence that the observed radiance, for a given illumination, is a function of the terrain orientation only. The reflectance map (Horn and Sjoberg, 1979) is best suited to describe and compute this function. On this basis and by using a digital terrain model to account for relief geometry, synthetic images were generated for applications such as image registration (Horn and Bachmann, 1978) and computer graphics (Horn, 1981). On the same basis, radiometric corrections were performed previously with isotropic (Sjoberg and Horn, 1980) and anisotropic (Smith *et al.*, 1980) reflection models. In practice, these methods are suited for satellite images.

This paper analyzes the more general case, typically encountered in low altitude imagery, where the assumption of parallel observation rays cannot be made and, consequently, the reflectance map cannot be used. A bidirectional reflection model is required. One such model results if we consider the terrain as a curved surface with an intrinsic reflectance characteristic. We analyze it for various analytical and numerical, isotropic and anisotropic reflection models for flat sites.

We also show its limits which leads us to the formulation of another, more general, model characterized by an orientation dependent reflectance characteristic. It turns out, however, to be beyond the limits of practical reflectance modeling.

As a practical approach to the correction of wide angle images of mountainous terrain, we finally suggest a model based on backscattering and diffuse reflection.

RADIOMETRIC ANALYSIS

This radiometric analysis is based on a remote sensing model and on several reflection models. It provides an exact description of the processes involved and explains main radiometric effects.

REMOTE SENSING MODEL

In order to present the reflection process on the ground in a wider context, we first consider a formal description of the complete remote sensing path.

To state the different factors which determine the sensitometry in remote sensing, let us consider

the model of Figure 1. The Earth's surface is illuminated by natural light on one hand and viewed by a light sensing system on the other hand. The light path, described from the source to the sensor, is as follows. We first consider the incident path with the top-of-the-atmosphere collimated light source of irradiance, E_0, produced by the sun. This light is attenuated and scattered inside the atmosphere. As a consequence, the illumination of the target has two basic components: direct attenuated sunlight and spatially distributed skylight. The direct sunlight is still a collimated beam, producing the attenuated irradiance, E_{01}, on a surface orthogonal to the light beam with the value

$$E_{01} = E_0 \cdot T_{a0}$$

where T_{a0} is the attenuation factor for the top-of-the-atmosphere irradiance, E_0. Because of foreshortening, the irradiance on the target produced by the direct beam is reduced to

$$E_{i1} = E_0 \cdot T_{a0} \cdot \cos\theta_{i0}$$

where θ_{i0} is the nadir angle of the sun incident beam (Figure 2).

The spatially distributed skylight can be characterized by a radiance function $L_{i2}(\theta_i,\phi_i)$ which produces an irradiance on the target according to

$$E_{i2} = \int_{-\pi}^{\pi} \int_{0}^{\pi/2} L_{i2}(\theta_i,\phi_i) \cdot \sin\theta_i \cdot \cos\theta_i \cdot d\theta_i \cdot d\phi_i$$

The total target irradiance is the sum of both components. It is written as

$$E_i = E_{i1} + E_{i2}$$

Next, the irradiated target reflects light in the whole hemisphere. The radiance, L_r, in the direction of the sensor depends on the target reflectance characteristic and the geometry of the incident and reflected beams. It is fully described by the bidirectional reflectance distribution function (BRDF), which is denoted by the symbol f_r and defined as
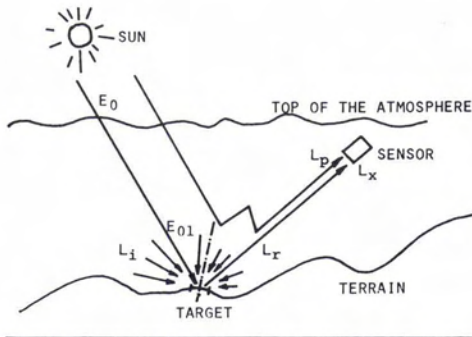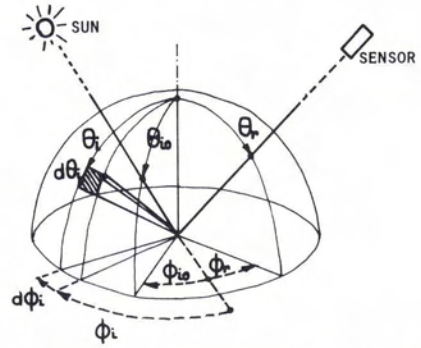

FIG. 2.   Spherical coordinate system bound to the target.

the ratio of reflected radiance, dL_r, in the direction of the sensor to the irradiance, dE_i, in the direction toward the source: i.e.,

$$f_r(\theta_i,\phi_i,\theta_r,\phi_r) = \frac{dL_r(\theta_i,\phi_i,\theta_r,\phi_r)}{dE_i(\theta_i,\phi_i)}$$

where θ_i and ϕ_i and θ_r and ϕ_r are respectively, the spherical angles of the incident and reflected beams in the target hemispherical coordinate system θ,ϕ (Figure 2). The radiance of a target with a given BRDF can thus be computed according to

$$L_r = \int_{hemisphere} f_r \cdot dE_i$$

Further along the light path, the reflected light beam, which extends from the target to the sensor, is again affected by the atmosphere. The radiance, L_x, measured by the sensor is the target radiance, L_r, attenuated by the factor, T_{ar}, plus an extra amount resulting from the scattered sunlight which is reflected toward the sensor all along the reflected beam path. The last is known as the path radiance L_p. Symbolically,

$$L_x = L_r \cdot T_{ar} + L_p.$$

Finally, there is the sensor path which leads from the radiance, L_x, entering the sensor to its digital value according to the sensor transfer function.

This concludes the description of the light path from the sun to the sensor. The atmosphere, the reflectance characteristic, and the sensor were shown to be the sensitometric factors in remote sensing. The correction of effects from the atmosphere and the sensor can be done by the methods mentioned in the introduction and is not treated in more detail here. The following sections concentrate on the estimation of the reflectance characteristic in the case of mountainous terrain.

TARGET GEOMETRY

Here we give a formal description of the light path geometry in a spherical coordinate system bound to the target.
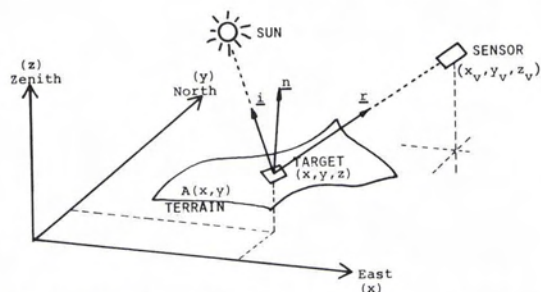

FIG. 1.   Remote sensing model.

FIG. 3. Terrain coordinate system with sun, target, and sensor.

FIG. 4. Target spherical coordinate system with main directions: sun (**i**), target normal (**n**), sensor (**r**), and highlight (**h**).

Figure 3 shows the target as an element of the Earth's surface $A(x,y)$ within the basic coordinate system x,y,z defined by the directions East, North, and Zenith, respectively. The vector **n*** normal to the target is obtained from the surface $A(x,y)$ with

$$\mathbf{n^*} = \left(-\frac{dA(x,y)}{dx}, \ -\frac{dA(x,y)}{dy}, \ 1 \right).$$

The direction of the illumination source is given by $\mathbf{i^*} = (x_i, y_i, z_i)$ and that of the viewer is obtained from the viewer location (x_r, y_r, z_r) by

$$\mathbf{r^*} = (x_v - x, \ y_v - y, \ z_r - z).$$

The unity vectors **n**, **i**, and **r** are obtained by normalizing **n***, **i***, and **r***, respectively.

Another important direction which will be used later is that of the highlight unit vector, **h**, which lies half way between **i** and **r**. Computationally,

$$\mathbf{h} = \frac{\mathbf{i} + \mathbf{r}}{|\mathbf{i} + \mathbf{r}|}.$$

Obviously, the highlight direction is constant for constant **i** and **r**. We can think of it as the direction resulting from **i** and **r** that the target normal must have in order to produce the largest specular reflection.

So far, these vectors are specified in the rectangular coordinate system x,y,z bound to the terrain. To perform the reflectance computation, their spherical coordinates in the target system (Figure 4) are needed. As coordinates, we will use here the cosine of the spherical angles which we call the M-variables. They are as follows:

For the incidence angle θ_i:

$$M_i = \cos \theta_i = \mathbf{n} \cdot \mathbf{i}.$$

For the reflection angle θ_r:

$$M_r = \cos \theta_r = \mathbf{n} \cdot \mathbf{r}.$$

For the phase angle α_p:
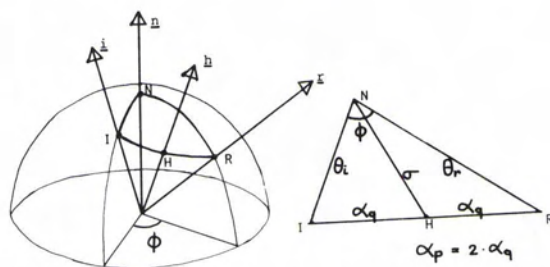
$$M_p = \cos \alpha_p = \mathbf{i} \cdot \mathbf{r}.$$

For the half phase angle $\alpha_q = \alpha_p/2$:

$$M_q = \cos \alpha_q = \mathbf{i} \cdot \mathbf{h} = \mathbf{r} \cdot \mathbf{h}.$$

For the azimuthal angle, ϕ, which is derived by using the cosine law for the spherical triangle θ_i, θ_r, and α_p (Figure 4), we have

$$M_f = \cos\phi = \frac{\cos\alpha_p - \cos\theta_i \cdot \cos\theta_r}{\sin\theta_i \cdot \sin\theta_r}.$$

Finally, for the off-specular angle σ:

$$M_s = \cos \sigma = \mathbf{n} \cdot \mathbf{h}.$$

This completes the characterization of the M-variables, which will now be used to formulate various reflection models with a common notation.

REFLECTION MODELS

The reflectance characteristic is fully described by the BRDF, and choosing a BRDF is identical to choosing a reflection model. The BRDF is, therefore, an ideal tool for comparing different reflection models. Here, typical known reflection models are formulated by their BRDF, which may be either in analytical or numerical form.

DIFFUSE MODEL

An ideal diffuser has a constant radiance, L_r, and reflects all incident light. Consequently, its BRDF is constant and its value is

$$f_{r,id} = \frac{1}{\pi}.$$

A real diffuser has a constant radiance, L_r, and, because of absorption, reflects the fractional part, ρ, of all the incident light. The value of its BRDF is

$$f_{r,d} = \frac{\rho}{\pi}.$$

TORRANCE-SPARROW'S SPECULAR MODEL

This model (Torrance and Sparrow, 1967) has proved to be very close to the reflection characteristic of shiny surfaces. As a result, it has become a

popular tool in computer graphics (Blinn, 1977). Its BRDF is modeled as consisting of a diffuse and a specular component; namely,

$$f_{r,ts} = k_s \cdot S + k_d$$

where k_d and k_s are model parameters defining the diffuse and specular proportions, respectively, and S is the specular function. This function is given by

$$S = \frac{D(M_s) \cdot F(M_q, n_i) \cdot G(M_s, M_r, M_i, M_q)}{M_i \cdot M_r}$$

when expressed with the M-variables. The functions D, F, and G are as follows. D is the microfacet distribution function which is typically

$$D(M_s) = M_s^{k_e}$$

where k_e is a model parameter permitting to specify the width of the specular highlight peak.

F is the Fresnel reflection function for the beam falling on a microfacet with a refraction index, n_i, under the angle of incidence, $\alpha_q = \arccos(M_q)$. Its value is

$$F(M_q, n_i) = \tfrac{1}{2}\left(\frac{b}{a}\right)^2 \cdot \left\{1 + \left(\frac{M_q \cdot a - 1}{M_q \cdot b - 1}\right)^2\right\}$$

where

$$a = \sqrt{n_i^2 + M_q^2 - 1} \quad +M_q^2$$
$$b = \sqrt{n_i^2 + M_q^2 - 1} \quad -M_q^2$$

Finally, G is an attenuation factor which captures the shadowing effects appearing at large incidence angles, θ_i, and large reflection angles, θ_r. Its value is

$$G(M_i, M_r, M_s, M_q) = \min\left\{1, \frac{2M_r \cdot M_s}{M_q}, \frac{2M_i \cdot M_s}{M_q}\right\}$$

This concludes the description of the Torrance-Sparrow BRDF as a function of the M-variables. The model itself is dependent on the model parameters, k_s and k_d; the exponent, k_e; and the refraction index, n_i.

HAPKE'S BACKSCATTERING MODEL

This model (Hapke, 1963) was especially developed to fit the BRDF of the moon, which is characterized by strong backscattering. Its BRDF is given by the expression

$$f_{r,h} = k_h \cdot f_{r,1}(M_i, M_r) \cdot B(\alpha_p) \cdot Z(\alpha_p)$$

where k_h is a scaling coefficient and the functions $f_{r,1}$, B, and Z are as follows: $f_{r,1}$ is the BRDF of the Lommel-Seelinger reflection law (Minnaert, 1961), whose expression is

$$f_{r,1} = \frac{1}{1 + \dfrac{M_r}{M_i}}$$

Its value does not vary much from 0.5 for a small incidence angle, θ_i, and reflection angle, θ_r, and its main merit in the Hapke's expression is to let the function become zero when θ_i is $\pi/2$.

Then, B is the retrodirective function responsible for the backscattering. Its form is

$$B(\alpha_p) = \begin{cases} \frac{1}{2} - \frac{1}{2t} \cdot (1 - e^{-t}) \cdot (3 - e^{-t}) & \text{if } \alpha_p \geq \pi/2 \\ & \text{else} \end{cases}$$

$$\text{where} \quad t = \frac{k_g}{t_q(\alpha_p)}$$

The parameter, k_g, is a means of controlling the width of the backscattering peak and is, therefore, also a model parameter.

Finally, the function, Z, is the scattering law of the surface. It is sometimes used as a means of changing the relative importance of forwardscattering and backscattering, but only under its form for increased backscattering does it have a physical justification. In this form its expression is

$$Z(\alpha_p) = \frac{\sin\alpha_p + (\pi - \alpha_p) \cdot \cos\alpha_p}{\pi}$$

To conclude, Hapke's BRDF is a function of the three variables M_i, M_r, and α_p. It is also dependent on the model parameters k_h and k_g and sometimes on the choice of the scattering law $Z(\alpha_p)$. These parameters permit one to fit the model to the actual surface behavior.

EGBERT'S MODEL

In this model (Egbert, 1977), a ground plane is considered covered with either spherical or cylindrical perturbations. The intrinsic surface of both the plane and the perturbations is supposed to be a Torrance-Sparrow reflector, i.e., to have a combined diffuse and specular reflection. Thus, the BRDF of Egbert's model is a sum of five terms: the diffuse and specular parts of both the plane and the perturbations, and the diffuse part of the shadows. The proportion of each term is fixed by coefficients which were experimentally shown to be essentially dependent on two parameters only: the density of the perturbations and their size.

NUMERICAL BRDF

Extensive measurements of natural surfaces have been done (Hapke, 1963; Eaton and Dirmhin, 1979; Kriebel, 1978; Kimes and Kirchner, 1981; Kimes et al., 1980) which can be used as a numerical BRDF. The exact measurement of the BRDF of a given surface is tedious because the BRDF is a function of four variables. Indeed, the measurement of a BRDF based, for example, on a spherical raster grid with a mesh of 10 degrees both on the incidence and on the reflection hemispheres requires $(36*8)^2 = 82944$ single measurements. This number is reduced by half by using the reciprocity

	SAND	MOON	SNOW	FOREST
Description:	diffuse surface	lunar surface	glazed snow	coniferous forest (λ = 580 nm)
Model:	diffuse	Hapke	Torrance & Sparrow	numerical
Parameters:	$f_{r,d}$= .6	k_g= .5	k_d= .6, k_s= 30 n_i=1.31, k_e=500	from [Kriebel]

FIG. 5.   Characterization of the four surfaces used in the simulation.

property of the BRDF (due to Helmholtz [Nicodemus *et al.*, date?]); i.e.,

$$f_r \ (\theta_i, \phi_i, \theta_r, \phi_r) = f_r \ (\theta_r, \phi_r, \theta_i, \phi_i).$$

This number is further reduced significantly by reducing the number of variables to three, assuming a rotational symmetry of the targets; i.e.,

$$f_{r,4} \ (\theta_i, \phi_i, \theta_r, \phi_r) = f_{r,3}(\theta_i, \theta_r, \phi)$$

where $ = \phi |\phi_i - \phi_r|$

Such an assumption is reasonable for most natural surfaces. Under these circumstances, the number in the above example is reduced to (8∗8∗19) = 1216, which is the number of single measurements required for determining the BRDF of a single target. It gives also the storage requirement for using it in a computer simulation. This number must be multiplied by the number of channels in multispectral applications.

FOUR MODELS COMPARED

In order to better understand their anisotropic behavior, we compare the shape of different reflection models. We choose to compare the shape

of their bidirectional reflectance distribution function (BRDF). The behavior of four typical surfaces, namely sand, lunar surface, glassy snow and forest, is now compared. The corresponding models as well as the parameters are summarized in Figure 5. These models all use the rotational invariance of the surface so that their BRDF are functions of three variables.

Figure 6 shows the BRDF of the four surfaces in the plane of incidence (ϕ = 0 and 180 degrees) as a function of the angle of reflection, θ_r, for several angles of incidence. These figures illustrate the strong anisotropies for which we are expected to make a correction.

RADIOMETRY IN THE IMAGE

In this section we analyze the main effect of reflectance anisotropy on the remotely sensed image, which manifests itself as a hot and specular spot, and the ways to avoid it.

REDUCING THE RADIANCE VARIATION IN THE IMAGE

Looking again at the curves of Figures 6 with the aim of avoiding the conditions which cause the
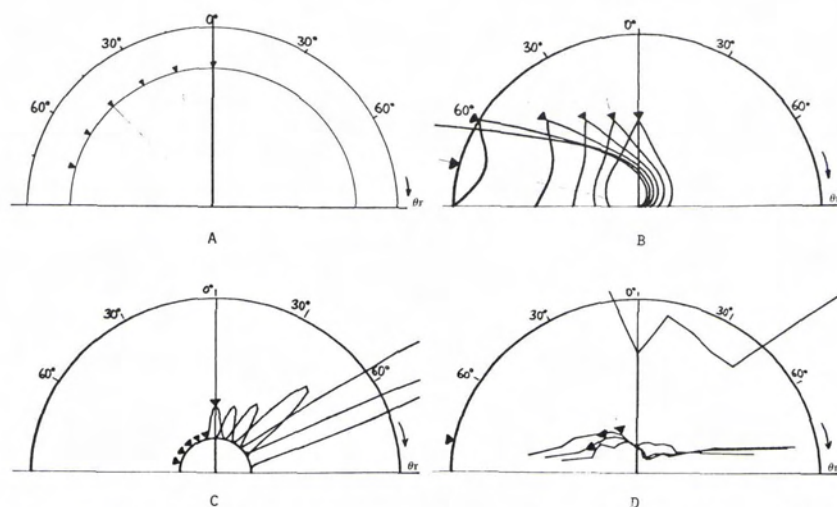

FIG. 6.   BRDF of four surfaces shown in the plane of incidence (ϕ = 0° and 180°) as a function of the reflection angle, θ_r. Several curves are shown corresponding to different incidence angles, θ_i, marked by an arrow.

strongest anisotropies, we see several regions to avoid:

- the specular and backscatter peaks, and
- the large angles of incidence θ_i and/or reflection θ_r.

The overall radiance variation of a given image can thus be significantly reduced by avoiding these zones of high anisotropy. This is done by choosing appropriate viewing and illumination conditions as will be shown. Before going on further in that direction, we give a formal description of the effect of the forwardscatter and backscatter peaks on the remotely sensed image.

HOT SPOT AND SPECULAR SPOT

The backscatter peak has its maximum when the phase angle, α_p, is zero (ref: Hapke's model), i.e., when the incident and reflected directions are identical; i.e.,

$$\mathbf{i} = \mathbf{r}.$$

Its effect on the image is a hot spot which lies on the straight line extending from the source through the sensor (Figure 7). This location, which is also called the antisolar point, has the particularity of being independent of the ground slope, i.e., it is located at the same place for flat and mountainous terrain (parallax not considered).

The forwardscatter peak shows its approximate maximum when the surface normal, $\mathbf{n}$, and the highlight vector, $\mathbf{h}$, are identical (ref: Torrance-Sparrow model) (the exact maximum being at an angle slightly lower than the angle for appropriate maximum):

$$\mathbf{h} = \mathbf{n} \quad , \text{i.e.,} \quad \theta_i = \theta_r \quad \text{and} \quad \phi = \pi.$$

According to this and for flat terrain, the resulting highlight or specular spot produced on the image is located in the plane of incidence (w,z) containing the sensor (Figure 7) and at a location symmetrical to the hot spot with respect to the sensor. In mountainous terrain, however, several specular spots are possible. They may appear all around the spot for flat terrain, provided that $\mathbf{h} = \mathbf{n}$. In order to describe their possible location in the plane of incidence, we assume a one-dimensional function, $A(w)$, describing the terrain in that plane. The terrain slope is

$$\tan\gamma = \frac{dA}{dW}$$

and simple geometry leads to the following condition (Figure 8):

$$\theta_r = \beta + \gamma$$

for the existence of a specular spot in the plane of incidence. Note that, with respect to the location
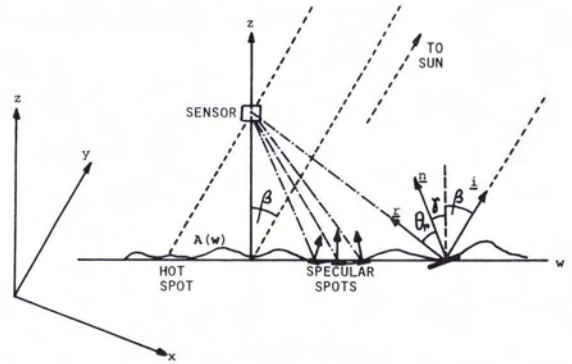

FIG. 7.   Hot spot and specular spots as viewed from the sensor.

of the specular spot for flat terrains, the possible locations in mountainous terrain are further from the viewer if the slope is toward the viewer and nearer if the slope is away from the viewer.

OPTIMAL VIEWING AND ILLUMINATION CONDITIONS

Returning to the appropriate choice of illumination and viewing conditions, we now see two favorable possibilities (Figure 8):

- A vertical viewing axis with a rather small viewing angle in order to avoid both types of spots. This also prevents large angles, θ_i and θ_r. The choice of the zenithal light source angle, β, is a trade off between keeping the light spots away from the viewer and avoiding large angles of incidence, θ_i.
- An oblique viewing axis to avoid both types of light spots with the same trade off for the choice of β. Here, however, we have the risk of θ_r becoming too large.

VISUAL SIMULATION AND MODEL GENERALIZATION

VISUAL SIMULATION

We now simulate the remote sensing process and generate synthetic views of both flat and mountainous terrain, in order to illustrate the combined effect of anisotropic reflectances and mountainous terrain. The elements required are basically a digital terrain model to describe the relief and a reflection model such as the ones described above.

The question arises as to how to combine the terrain model and the reflection model. The present simulation is based on the assumption that the surface reflectance characteristic of the terrain is constant, i.e., it is both space and slope invariant. This assumption is the key to the generation of synthetic views which then comprises the following steps: (a) defining the light
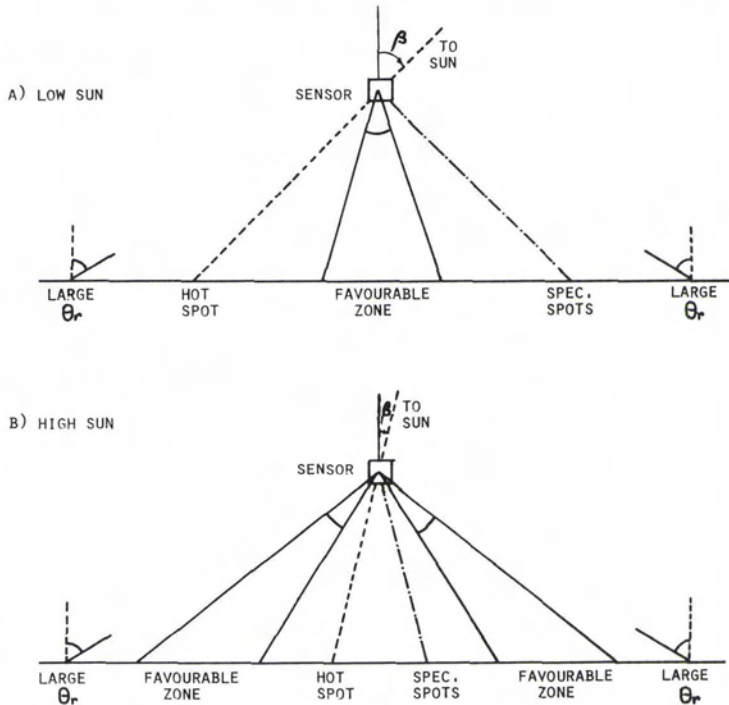
FIG. 8. Favorable viewing conditions which avoid the areas of strongest anisotropies.

source vector, **i**, which is constant for the entire image; (b) using the location of the sensor and the digital terrain model to determine the value of the directions, **n** and **r**, for each pixel; (c) transforming **i**, **n**, and **r** in *M*-variables; and, finally, (d) computing the image luminance according to the four different reflection models.

The present simulation uses a digital terrain model derived from the U.S. Geological Survey. We use the site of Redondo Peak, New Mexico with a size of 15.5 km by 15.5 km that encompasses 256 by 256 elevation elements equally spaced on a rectangular grid. As reflection models, we will consider the four models previously described which stand for sand, moon, snow, and forest, respectively.

Figure 9 shows the results of the simulation. Shown are vertical views on both a flat (Figure 9(1)) and a mountainous (Figures 9(2), 9(3), and 9(4)) terrain which reflect light according to the four reflection models. In all images North is on top, and the illumination is from South-West at an incidence angle of 55 degrees. For different images the sensor is located at different distances from the ground and the viewing angle is adjusted in order to depict the same part of the terrain. In Figure 9(2) the mountainous terrain is viewed from a geostationary orbit under a viewing angle of 0.02 degrees. The terrain of both Figures 9(1) and

9(3) is viewed from an identical altitude of 25,000 feet. In order to facilitate the comparison between images 9(1) and 9(3), the flat terrain was choosen to lie at the mean altitude of the mountainous terrain, i.e., 8000 feet. Using this mean altitude, a viewing angle of 112 degrees is determined. As for Figure 9(4), this is an extreme case where the terrain is viewed from an altitude of 15,000 feet, which results in a mean viewing angle of 145 degrees.

These images demonstrate the effect of anisotropic BRDF on the overall radiometry of the resulting images. The isotropic sand model serves as a reference, and its images are, of course, unchanged in the different views. The moon model gives rise to a very strong hot spot whose location, as expected, is different in each image. With the snow model, the typical behavior of a shiny surface characterized by several terrain-orientation-dependent specular spots or highlights is found. Finally, the forest model also produces important radiometric changes in the images, which are less easy to interpret however.

The images resulting from the numerical forest model suggest the following comments. First, the image of the flat terrain reveals a rough quantization of the numerical BRDF. Although the values are computed from the numerical BRDF by means of a linear interpolation, important radiometric
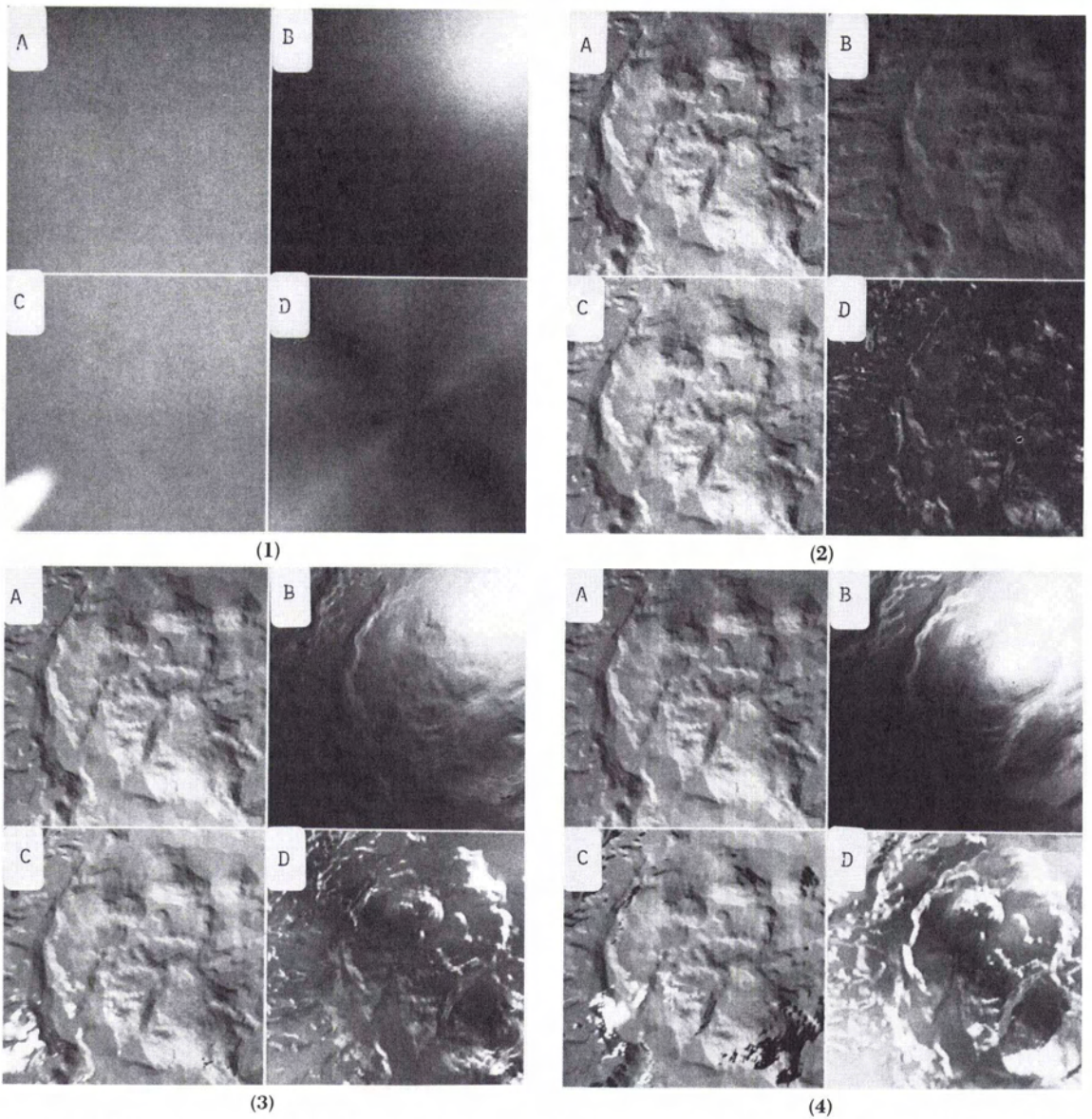
FIG. 9.   Simulated views of a flat and mountainous terrain according to four different reflection models: (A) sand, (B) moon, (C) snow, and (D) forest. (1) Flat terrain viewed from a 25,000-foot altitude; (2) mountainous terrain viewed from an infinite altitude; (3) mountainous terrain viewed from a 25,000-foot altitude; and (4) mountainous terrain viewed from a 15,000-foot altitude.

variations are visible, which suggest that a more accurate model is needed if radiometric corrections are to be performed on this basis.

Second, a closer look at the forest images of Figures 9(2), 9(3), and 9(4) reveals an important increase in the overall luminance when the viewer distance to the terrain increases. This is well explained by the corresponding increase of the reflection angles of the single pixels. Another visible effect is the strong luminance variation as a func-

tion of the surface orientation in the mountainous terrain. This variation is in fact much more important for the forest than the corresponding variation in the diffuse model. We have to explain this phenomenon which does not correspond to what we really see in images from forests in mountainous terrain. A pertinent explanation is that the basic assumption we made for this simulation is not valid and that a different description of the reflection is required in mountainous terrain.
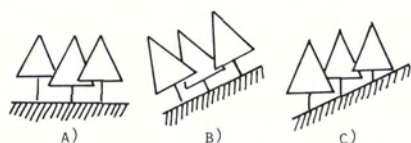
FIG. 10. Assumed structure of the ground for different reflection models.

GENERALIZED MODEL

The results of the simulation suggest that a model based on a surface spanned on the relief with an intrinsic orientation-invariant BRDF does not hold, at least for forest cover. This suggestion will now be reinforced by the following explanation of the real meaning of this assumption:

Let us consider a surface covered with forest. In the case of a flat site as shown in Figure 10a, the BRDF is

$$f_r = f_r(\theta_i, \theta_r, \phi)$$

where
θ_i = constant,
$\theta_r = \theta_r(x, y)$, and
$\phi = \phi(x, y)$.

The case of the mountainous site, where the assumption of a constant BRDF is made, is shown in Figure 10b and is described by the following orientation invariant BRDF:

$$f_r = f_r(\theta_i, \theta_r, \phi)$$

where
$$\theta_i = \theta_i\left(\frac{dA}{dx}, \frac{dA}{dy}\right),$$

$$\theta_r = \theta_r\left(x, y, \frac{dA}{dx}, \frac{dA}{dy}\right), \text{ and}$$

$$\phi = \phi\left(x, y, \frac{dA}{dx}, \frac{dA}{dy}\right).$$

The invariance assumed in this case would imply that trees grow perpendicular to the tilted surface, which is obviously not the case. This explains the phenomenon observed before in the simulated images and suggests also that such a model is unable to describe the exact behavior of vegetated surfaces with variable orientation.

A more general model is thus required to describe the reflection of the surface of Figure 10c. An orientation-dependent BRDF makes this possible: i.e.,

$$f_r = f_r\left(\theta_i, \theta_r, \phi, \frac{dA}{dx}, \frac{dA}{dy}\right)$$

where θ_i, θ_r, and ϕ are as above.

PRACTICAL LIMITS OF REFLECTION MODELING

With a five-variable BRDF like the above, we reach the reasonable practical limits of reflection modeling. This is particularly true when working with numerical BRDFs, in which case the determination of the model alone would require a prohibitive amount of measurements. But this is also true if an analytical BRDF is used (assuming that such a model can be found), because here, also, its determination would require very tedious measurements.

Above all, it is doubtful that such a very precise model can really be used. This is because the vegetated surfaces in mountainous terrain lack the relative homogeneity encountered in flat terrain, so that a very precise model is not really worthwhile.

PRACTICAL CORRECTION METHOD

We will now suggest a more practical approach for the radiometric correction of airborne remotely sensed images. Because of the difficulty mentioned above of defining an exact model of reflection, we will concentrate on the correction of the major radiometric inhomogeneities in the image.

In remotely sensed images from mountainous terrain, the most obvious radiometric variations caused by illumination and viewing angles are the consequence of (a) foreshortening and (b) backscattering. Foreshortening describes the variation of the effective surface of the target when its orientation changes. This effect is considered in the diffuse reflection model. On the other hand, backscattering is obvious on vegetated surfaces. Even if it is less strong, it is somewhat comparable to the backscattering of the lunar surface.

These considerations allow us to propose the following practical BRDF built on the BRDFs of both the diffuse model $(f_{r,d})$ and Hapke's model $(f_{r,h})$:

$$f_r = k_d' \cdot f_{r,d} + k_h \cdot f_{r,h}$$

or

$$f_r = k_d + k_h \cdot f_{r,d}$$

where k_d and k_h are scaling parameters. Their value must be adjusted in order to obtain a best fit between the real recorded image and the synthetic correction image generated with this rule and using the appropriate digital terrain model. Note that, with this model, the resulting radiance in the image has a terrain-variable component, the diffuse, and a roughly terrain-invariant component, the backscattering. This facilitates the parameter adjustment. Practical results based on this model can be found in a separate paper (Shibata et al., 1981).

CONCLUSION

We have reviewed the mechanisms of reflection in the case of natural surfaces in mountainous ter-

rain, and demonstrated their effect on the radiometry of remotely sensed images. Using the reflection characteristics of sand, lunar surface, snow, and forest, simulated images of mountainous terrain were generated based on the assumption of a surface with an intrinsic orientation-invariant reflection characteristic. This approach was shown to be feasible only for simple flat surface covers. Surfaces with an important vertical structure such as vegetated surfaces and especially forests require a more complex reflection model in which the BRDF is also a function of the surface orientation. For practical purposes, however, a more simple reflection model is proposed, which permits one to compensate well major radiometric effects of airborne remotely sensed images of mountainous terrain.

REFERENCES

Ahern, F., P. M. Teillet, and D. G. Goodenough, 1978. Transformation of Atmospheric and Solar Illumination Conditions on the CCRS Image Analysis System, *Machine Processing of Remotely Sensed Data Symp.*, pp. 34-52.

Allen, W. A., T. V. Gayle, and A. J. Richardson, 1970. "Plant-Canopy Irradiance Specified by the Duntley Equations", *Journal Optical Society of America*, Vol. 60, No. 3, pp. 372-376.

Blinn, J. F., 1977. Models of Light Reflection for Computer Synthesized Pictures, *Computer Graphics*, Vol. 11, pp. 192-198.

Divari, N. B., 1970. *Atmospheric Optics*, Consultant Bureau, N.Y., (transl. from Russian).

Eaton, F. D., and I. Dirmhin, 1979. Reflected Irradiance Indicatrices of Natural Surfaces and their Effect on Albedo, *Applied Optics*, Vol. 18, No. 7, pp. 994-1008.

Egbert, D. D., 1977. A Practical Method for Correcting Bidirectional Reflectance Variations, *Machine Processing of Remotely Sensed Data Symposium*, pp. 178-189.

Favre, Herman M., P. Y. Deschamps, and A. de Leffe, 1979. Atmospheric Modeling for Space Measurement of Ground Reflectances, Including Bidirectional Properties, *Applied Optics*, Vol. 18, No. 21.

Frei W., M. Singh, and T. Shibata, 1980. Digital Image Change Detection, *SPIE Optical Engineering*, Vol. 19, No. 3, pp. 331-338.

Hapke, B. W., 1963. A Theoretical Photometric Function for the Lunar Surface, *Journal of Geophysical Research*, Vol. 68, No. 15, pp. 4571-4586.

Hapke, B., and H. Van Horn, 1963. Photometric Studies of Complex Surfaces, with Applications to the Moon, *Journal of Geophysical Research*, Vol. 68, No. 15, pp. 4545-4570.

Holben, B. N., and C. O. Justice, 1980. The Topographic Effect on Spectral from Nadir-Point Sensors, *Photogrammetric Engineering and Remote Sensing*, Vol. 46, No. 9, pp. 1191-1200.

Horn, B. K. P., 1981. Hill Shading and the Reflectance Map, *Proc. IEEE*, Vol. 69, No. 1, pp. 14-47.

Horn, B. K. P., and B. L. Bachmann, 1978. Using Synthetic Images to Register Real Images with Surface Models, *C.A.C.M.*, Vol. 21, No. 11, pp. 914-924.

Horn, B. K. P., and R. W. Sjoberg, 1979. Calculating the Reflectance Map, *Applied Optics*, Vol. 18, No. 11, pp. 1770-1779.

Kimes, D. S., and J. A. Kirchner, 1981. Modeling the Effects of Various Radiant Transfers in Mountainous Terrain on Sensor Response, *IEEE Transactions on Geoscience and Remote Sensing*, Vol. 19, No. 2, pp. 100-108.

Kimes, D. S., J. A. Smith, and K. J. Ranson, 1980. Vegetation Reflectance Measurements as a Function of Solar Zenith Angle, *Photogrammetric Engineering and Remote Sensing*, Vol. 46, No. 12, pp. 1563-1573.

Koepke, P., and K. T. Kreibel, 1978. Influence of Measured Reflection Properties of Vegetated Surfaces on Atmospheric Radiance and its Polarization, *Applied Optics*, Vol. 17, No. 2, pp. 260-264.

Kriebel, K. T., 1978. Measured Spectral Bidirectional Reflection Properties of Four Vegetated Surfaces, *Applied Optics*, Vol. 17, No. 2, pp. 253-259.

Lintz, J. Jr., and D. S. Simonett, 1976. *Remote Sensing of Environment*, Addison Wesley Publishing Company, Massachusetts.

Middleton, W. E. K., and A. G. Mungall, 1972. The Luminous Directional Reflectance of Snow, *Journal Optical Society of America*, Vol. 42, No. 8, pp. 572-579.

Minnaert, M., 1961. Photometry of the Moon, in *The Solar System, III, Planets and Satellites*, by Kniper G. P. and Middlehurst B. M., Chicago, pp. 213-248.

Nagao, Makoto, 1977. Low Level Processing for Aerial Photograph Analysis, *U.S.-Japan Seminar on Robot Vision*, Cambridge Mass.

Nicodemus, F. E., J. C. Richmond, and J. J. Hsia, 1977. *Geometrical Considerations and Nomenclature for Reflectance*, National Bureau of Standards, Monograph 160.

RCA, 1974. *Electro-Optics Handbook*, RCA. 1974

Reeves, R. G., A. Anson, and D. Landen, 1975. *Manual of Remote Sensing*, American Society of Photogrammetry, Falls Church, Virginia.

Richason, B. F., 1978. *Laboratory Manual for Introduction to Remote Sensing of the Environment*, Kendall, Hunt Publishing Company, Dubuque Iowa.

Robinove, Ch. J., and P. S. Chavez, Jr., 1978. Landsat Albedo Monitoring Method from an Arid Region, *AAAS Int. Symp. on Arid Region Plant Resources*, Lubbock, Texas.

Shibata, T., W. Frei, and M. Sutton, 1981. Digital Correction of Solar Illumination and Viewing Angle Ar-

tifacts in Remotely Sensed Images, *Proc. Machine Processing of Remotely Sensed Data Symposium.*

Sjoberg, R. W., and B. K. P. Horn, 1980. Atmospheric Modelling for the Generation of Albedo Images, *Proc. Image Understanding Workshop,* DARPA, Maryland.

Smith, J. A., T. L. Lin, and K. J. Ranson, 1980. The Lambertian Assumption and Landsat Data, *Photogrammetric Engineering and Remote Sensing,* Vol. 46, No. 9, pp. 1183-1189.

Suits, G. H., 1972. The Calculation of the Directional Reflectance of a Vegetative Canopy, *Remote Sensing of Environment,* Vol. 2, pp. 117-125.

Torrance, K. E., and E. M. Sparrow, 1967. Theory for Off-Specular Reflection from Roughened Surfaces,

Journal Optical Society of America, Vol. 57, No. 9, pp. 1105-1114.

Tricker, R. A. R., 1970. *Introduction to Meteorological Optics,* American Elsevier Publishing Company Inc., N.Y.

Trowbridge, T. S., and K. P. Reitz, 1975. Average Irregularity Representation of a Rough Surface for Ray Reflection, *Journal Optical Society of America,* Vol. 65, No. 5, pp. 531-536.

Walker, J. E., 1979. Photometry: Linking Earth, Air and Analysis, *Optical Spectra,* Vol. 13, Issue 8.

World Conference on
Engineering and Engineering Technology Education

Cologne, Federal Republic of Germany
16-20 April 1984

This Conference—under the patronage of the President of the Federal Republic of Germany and organized by the Fachhochschule Köln in cooperation with UNESCO—has as its aim to make a world wide presentation of the different educational programs and to present specific examples of the types of activities and courses of these institutions. Papers on the educational technical nature as well as on the administrative aspects of the management of educational programs are called for. It is also proposed to consider the level of academic attainment required for a successful integration of the engineering graduate in industry, and the need for attaining a more uniform standard for engineering and engineering technology graduates.

For further information please contact

Dr. Beaumont Davison, Dean of Engineering
California State Polytechnic University
3801 West Temple Avenue
Pomona, CA 91768